European Journal of Pharmaceutics and Biopharmaceutics 172 (2022) 134–143

Contents lists available at ScienceDirect

European Journal of Pharmaceutics and Biopharmaceutics

journal homepage: www.elsevier.com/locate/ejpb

# Incorporation of phosphatidylserine improves efficiency of lipid based gene delivery systems

Claudia. Lotter [a,1], Claudio. Luca. Alter [a,b,1], Jan. Stephan. Bolten [a], Pascal. Detampel [a], Cornelia. G. Palivan [b,c], Tomaž. Einfalt [a,2], Jörg. Huwyler [a,*,2]

[a] Department of Pharmaceutical Sciences, Division of Pharmaceutical Technology, University of Basel, Klingelbergstrasse 50, 4056 Basel, Switzerland
[b] Swiss Nanoscience Institute, University of Basel, Klingelbergstrasse 82, 4056 Basel, Switzerland
[c] Department of Chemistry, University of Basel, Mattenstrasse 24a, BPR 1096, 4003 Basel, Switzerland

ARTICLE INFO

*Keywords:*
Lipid nanoparticles
Nucleic acid delivery
Transfection efficiency
Transfection potency
Lipid composition
Phosphatidylserine

ABSTRACT

The essential homeostatic process of dead cell clearance (efferocytosis) is used by viruses in an act of apoptotic mimicry. Among others, virions leverage phosphatidylserine (PS) as an essential "eat me" signal in viral envelopes to increase their infectivity. In a virus-inspired biomimetic approach, we demonstrate that PS can be incorporated into non-viral lipid nanoparticle (LNP) pDNA/mRNA constructs to enhance cellular transfection. The inclusion of the bioactive PS leads to an increased ability of LNPs to deliver nucleic acids *in vitro* to cultured HuH-7 hepatocellular carcinoma cells resulting in a 6-fold enhanced expression of a transgene. Optimal PS concentrations are in the range of 2.5 to 5% of total lipids. PS-decorated mRNA-LNPs show a 5.2-fold enhancement of *in vivo* transfection efficiency as compared to mRNA-LNPs devoid of PS. Effects were less pronounced for PS-decorated pDNA-LNPs (3.2-fold increase). Incorporation of small, defined amounts of PS into gene delivery vectors opens new avenues for efficient gene therapy and can be easily extended to other therapeutic systems.

## 1. Introduction

There is a growing interest in solid lipid nanoparticles (LNPs) as a drug delivery system for nucleic acids. The FDA approval in 2018 of the first LNP based siRNA drug (Patisiran) and the worldwide approval of COVID-19 mRNA LNP based vaccines were the first clinical applications of LNPs for non-viral nucleic acid therapy [1,2]. Classic LNP formulations are composed of charged lipids and lipid-like adjuvants. Cationic lipids bind and condense the negatively charged nucleic acids. This is a prerequisite to enable cellular uptake and subsequently their release from the endosomal compartment to the cytoplasm. Due to the high systemic toxicity and poor pharmacokinetic properties of permanently charged cationic LNPs [3,4], current clinically translated LNP therapies are based on ionizable lipids. The chemical nature of ionizable lipids with a $pK_a$ around 6.7 (i.e. 1,2-dioleyloxy-3-(dimethylamino)propane (DODMA)) can be leveraged to formulate pH-responsive LNPs [5,6]. In this regard, extensive chemical optimization of ionizable lipids has been conducted to improve the delivery efficiency of LNPs [7,8]. Besides charged lipids, additional "helper lipids" are needed for the formation of solid nanoparticles. Altering the helper lipid composition of LNP formulations reduces their cytotoxicity and leads to increased potencies *in vitro* and *in vivo* [9–15]. For example, it has been shown that the

*Abbreviations:* CLSM, confocal laser scanning microscopy; $D_H$, hydrodynamic diameter; DLS, dynamic light scattering; DODMA, 1,2-dioleyloxy-3-(dimethylamino) propane; DOPC, 1,2-dioleoyl-*sn*-glycero-3-phosphocholine; DOTAP, 2,3-dioleoyloxy-propyl-trimethylammoniumchlorid; DMPE-PEG2000, 1,2-dimyristoyl-*sn*-glycero-3-phosphoethanolamine-N-[methoxy (polyethylene glycol)-2000; EE, encapsulation efficiency; EGFP, enhanced green fluorescent protein; i.v, intravenous; hpi, hours post injection; LNP, lipid nanoparticle; mRNA, messenger RNA; MTS, 3-(4,5-dimethylthiazol-2-yl)-5-(3-carboxymethoxyphenyl)-2-(4-sulfophenyl)–2H-tetrazolium; N/P, lipid-nitrogen (N) to oligonucleotide-phosphate (P) ratio; PDI, polydispersity index; pDNA, plasmid DNA; PEG, polyethylene glycol; PS, L–α–phosphatidylserine; TE, transfection efficiency, number of EGFP positive cells; TP, transfection potency, mean EGFP signal intensity expressed as single-cell relative fluorescence units; ZFE, zebrafish embryo.

* Corresponding author at: Department of Pharmaceutical Sciences, University of Basel, Klingelbergstrasse 50, CH-4056 Basel, Switzerland.
*E-mail address:* joerg.huwyler@unibas.ch (Jörg. Huwyler).

[1] Contributed equally.
[2] T.E. and J.H. have contributed equally to this work as senior last authors.

https://doi.org/10.1016/j.ejpb.2022.02.007
Received 5 November 2021; Received in revised form 11 February 2022; Accepted 11 February 2022
Available online 15 February 2022

implementation of specific polyethylene glycol-functionalized (PEG) lipids can control the circulation time and influence LNP biodistribution [9,10]. The replacement of the classical cholesterol with bioactive phytosterols has been proven to alter the morphology, the internalization mechanisms, and the subcellular trafficking of LNPs [11–14]. Similarly, with the substitution of the helper lipid 1,2-distearoyl-*sn*-glycero-3-phosphocholine (DSPC) with 1,2-dioleoyl-*sn*-glycero-3-phosphocholine (DOPC) or 1-stearoyl-2-oleoyl-*sn*-glycero-3-phosphocholine (SOPC), a notable increase in LNP effectiveness has been achieved [13,14]. Furthermore, the substitution of DSPC by unsaturated PCs had a strong impact on transfection efficiency and toxicity of LNPs although effects were different for LNP-siRNA and LNP-pDNA systems [13].

Despite all of these efforts, the efficiency of LNP based formulations is still suboptimal and not comparable to the one of viral vectors. Unlike LNPs, viral envelopes have complex lipidomic compositions [16]. In the present study, we introduce a new strategy to improve the LNP efficacy that is inspired by virus envelopes. In particular, we focus on the bioactive phospholipid phosphatidylserine (PS) [17], which affects cellular internalization and intracellular processing. We selected PS as it represents an essential co-factor during the infection process of several viral types [18–20], including the Ebola, Epstein Barr, and Hepatitis B virus [21]. By inclusion of PS in their membranes, virions camouflage themselves as dead cells in an act referred to as apoptotic cell mimicry [21]. In mammalian cells, PS is actively kept on the inner leaflet of the cellular membrane by the flippase enzyme family. However, through the induction of apoptosis or necrosis, PS gets gradually exposed to the outer leaflet. This in turn induces PS recognition and apoptotic cell clearance. This process called efferocytosis is highly evolutionarily conserved due to the constant turnover of cells [22,23]. Efferocytosis is performed by both professional (i.e. macrophages) and non-professional phagocytes (i.e. tissue cells) [22,24,25]. The key receptor families to which PS has been reported to bind include G-protein-coupled TIM (TIM1, TIM3, TIM4) and TAM (Gas6, ProS) receptors [26]. Surface presentation of PS and interaction with TIM receptors is also exploited by other parasitic organisms [27] and is an essential bioactive molecule in the entry of exosomes [28–30]. Furthermore, PS bearing liposomes were previously demonstrated to effectively alter subcellular trafficking of liposomes to the endoplasmic reticulum of non-phagocytic cells in a viral-like manner [31].

It was therefore the aim of the present study to explore whether the decoration of LNPs with PS increases transfection. We incorporated PS in both cationic and ionizable LNPs. Using optimized lipid-nitrogen to oligonucleotide-phosphate (N/P) ratios, we used a screening approach to design PS-decorated LNPs with desired physico-chemical properties such as particle size and size distribution, surface charge, and nucleic acid condensation efficiency. Mechanistic studies were used to investigate the impact of PS on transfection efficiency (TE) as well as transfection potency (TP), cellular LNP uptake, viability, and subcellular trafficking of LNPs. Uptake and cellular processing of both pDNA and mRNA encoding for an enhanced green fluorescent protein transgene (EGFP) were studied. Lead PS-LNPs formulations were tested with respect to TP and TE *in vivo* in a vertebrate zebrafish embryo (ZFE) model (Fig. 1).

## 2. Material and methods

### 2.1. Materials and chemicals

1,2-dioleyloxy-3-dimethylaminopropane (DODMA), 1,2-dioleoyl-*sn*-glycero-3-phosphocholine (DOPC), L-α-phosphatidylserine (brain derived PS), 1,2-dimyristoyl-*sn*-glycero-3-phosphoethanolamine-N-[methoxy(polyethylene glycol)-2000] (DMPE-PEG200) were purchased from Avanti Polar Lipids (Alabaster, AL). 2,3-dioleoyloxy-propyl-trimethylammoniumchlorid (DOTAP) was purchased from Corden Pharma (Frankfurt am Main, Germany). Cholesterol, DiI, Hoechst 33342 and 7-Aminoactinomycin D (7-AAD) were obtained from Sigma Aldrich (Schaffhausen, Switzerland). SYBR Gold Nucleic Acid Gel Stain (SYBR gold reagent), DiO, Chloropromazine, Polyinosinic acid (Poly I), Colchicine, Nystatin and Dynasore were acquired by Thermo Fisher Scienctific (Zug, Switzerland). AnnexinV was purchased from Biolegend (San Diego, CA), Label IT Cy5 Kit from Mirus Bio (Madison, WI) and Chol-PEG-FITC-5k from Nanocs (New York, NY). The minicircle plasmid DNA encoding for EGFP under the control of a liver-specific p3 promoter [32] was kindly provided by the University Children's Hospital Zurich.

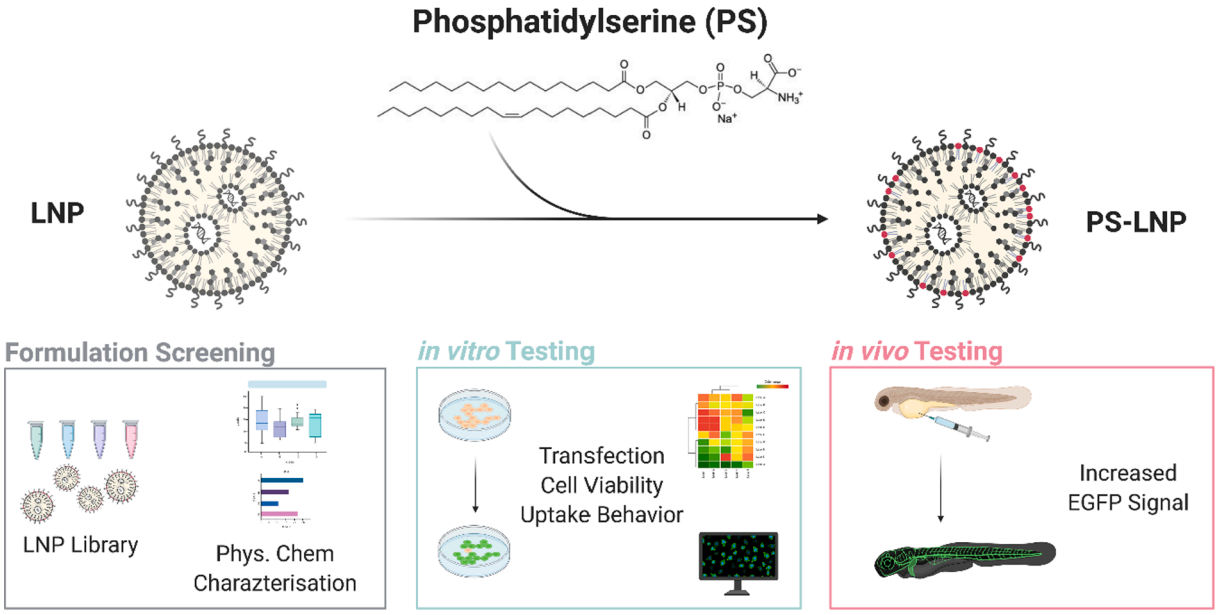


**Fig. 1.** Design and evaluation of lipid nanoparticles (LNPs) equipped with phosphatidylserine (PS). LNPs were formulated with PS, DOPC, and cholesterol as helper lipids and DOTAP or DODMA as cationic or ionizable nucleic acid condensation agents, respectively. PS-LNPs had a defined hydrodynamic diameter and ζ-potential. Cellular uptake, transfection potency, and transfection efficiency of PS-LNPs were evaluated *in vitro* (i.e., HuH-7 hepatic carcinoma cell line) as well as *in vivo* (i.e., zebrafish embryo). EGFP: enhanced green fluorescent protein transgene. (For interpretation of the references to color in this figure legend, the reader is referred to the web version of this article.)

NTC9385R (3xCpG)-CAG EGFP-CpG free BGH pA nanovector plasmid DNA was obtained from Nature Technology Corp (Lincoln, NE). Minicircle plasmid DNA used for *in vitro* experiments and nanovector plasmid DNA used for *in vivo* experiments are referred to as pDNA. 5′ capped CleanCap EGFP mRNA was purchased from TriLink Biotechnologies (San Diego, CA). Dulbecco's modified Eagle's medium (DMEM) high glucose (4500 mg $L^{-1}$) was obtained from Sigma Aldrich and supplemented with 10% FCS (BioConcept, Allschwil, Switzerland), penicillin (100 units $mL^{-1}$), and streptomycin (100 μg $mL^{-1}$) (Sigma Aldrich). Trypsin/EDTA (0.25%) was purchased from Gibco. FACS buffer, composed of DPBS (Sigma Aldrich), was supplemented with 1% FCS, 2.5 mM EDTA, 0.05% $NaN_3$.

### 2.2. Preparation of LNPs

Lipid nanoparticles used for *in vitro* experiments were prepared using a bulk mixing method as described elsewhere [32]. Briefly, lipid solutions (DODMA/DOTAP, Cholesterol, DOPC and PS at molar ratios of 50:40:10:0, 50:40:9.5:0.5, 50:40:9:1, 50:40:7.5:2.5, 50:40:5:5 and 50:30:20:10) were solved in $CHCl_3$, taken to dryness by rotational evaporation under reduced pressure for 1 h and rehydrated using 5% glucose, 20 mM sodium acetate, pH 4 (LNP sample buffer). The final lipid concentration was 0.8 mM. Liposomes were extruded 13 times using a manual mini extruder (Avanti Polar Lipids) and polycarbonate membranes (Nucleopore, Whatman, North Bend, OH) with a pore size of 100 nm. For LNP complexation with pDNA or mRNA, LNPs were combined at the desired N/P ratio with nucleic acids solved in LNP sample buffer. They were incubated at 22 °C for 30 min at 300 rpm. For *in vivo* experiments, LNPs containing PEGylated lipids were used. The lipid composition was DODMA:Cholesterol:DOPC:DMPE-PEG2000 = 50:39:10:1. Where indicated, DOPC was partially substituted with PS to reach the indicated final percentage of this lipid. The total amount of DOPC and PS was 10% of total lipids. The dry film was rehydrated at 70 °C using methanol:ethanol = 20:80. The lipid solution (organic phase) was combined with the nucleic acids solved in LNP sample buffer (aqueous phase) at the desired N/P ratio by microfluidics (NanoAssemblr; Precision Nanosystems, San Jose, CA). Flow rate was 20 mL $min^{-1}$ with an organic:aqueous phase ratio of 1:3. Buffer was exchanged at 4 °C to 0.9% NaCl, 1 mM HEPES, at pH 7.4 (*in vivo* sample buffer) by dialysis (Millipore, 12,000–14,000 molecular weight cut-off). Dialyzed samples were collected and characterized by a nucleic acid exclusion assay using SYBR gold reagent. Where indicated, LNPs were labeled with fluorescent dyes. No particle aggregation was observed upon storage at 4 °C for at least one week. For all experiments, only freshly prepared LNPs were used. All formulations showed colloidal stability.

### 2.3. LNP size, size distribution and ζ-potential

PS-LNP size distribution and ζ-potential were determined by dynamic light scattering using a Zetasizer Ultra (Malvern Panalytical, Volketswil, Switzerland). For ζ-potential measurement: PS-LNPs were diluted 1:40 in either LNP sample buffer or 5% glucose/10 mM HEPES, pH 7.4.

### 2.4. Evaluation of nucleic acid encapsulation efficiency

The encapsulation efficiency (EE) of the particles was determined by a nucleic acid exclusion assay using SYBR gold reagent. Briefly, 190 μL diluted fluorescent dye was added to 10 μL LNP solution in the presence or absence of 0.2% (w/v) Triton-X100 and incubated for 5 min. A linear calibration curve was obtained for each of the tested nucleic acids. Fluorescence was measured at $\lambda_{ex} = 485$ nm, $\lambda_{em} = 530$ nm and $\lambda_{Cutoff} = 515$ nm.

### 2.5. Cell culture

HuH-7 cells were obtained from American Type Culture Collection (ATCC, Manassas, VA) and cultured in DMEM (55 $cm^2$ dishes, 37 °C, 5% $CO_2$, saturated humidity). The cells were harvested at 80% confluency.

### 2.6. Flow cytometry

$2 \times 10^4$ HuH-7 cells were seeded onto Collagen (Collagen I, rat tail) coated 24-well plates and allowed to adhere overnight. Cell medium was removed, cells were trypsinized for 5 min and further uptake was blocked by addition of 300 μL FACS buffer containing 7-AAD (2 μg $mL^{-1}$) at least 20 min prior use. Samples were kept on ice until analyzed. Experiments were analyzed by flow cytometry using a FACS Canto II (BD Bioscience, San Jose, CA). Doublets were excluded using FSC-A and SSC-A detectors. The apoptotic cells were excluded using FL2-A (695/40). A total of 10′000 single cells for each sample were analyzed and data were processed using Flow Jo VX software (TreeStar, Ashland, OR).

### 2.7. In vitro transfection experiments

In these experiments, "transfection efficiency" (TE) refers to the number of transfected cells. "Transfection potency" (TP) refers to the mean signal intensity of the whole cell population expressed in terms of relative fluorescent units. Cells were incubated with 100 μL PS-LNPs for 48 h for pDNA and 24 h for mRNA in 500 μL DMEM at the indicated final nucleic acid concentrations/well (0.28 μg $mL^{-1}$ or 0.83 μg $mL^{-1}$). TE and EGFP signal intensity in cells were analyzed using flow cytometry. A TE value of 100% thereby would indicate that 100% (number) of target cells were transfected. Furthermore, a normalized signal intensity value of 100% refers to the highest observed median EGFP signal in a given experiment.

### 2.8. Time dependent uptake

100 μL PS-LNPs condensing a mixture of 1:4 Cy5-labeled nucleic acid:non-labeled nucleic acid were added to HuH-7 cells at a final nucleic acid concentration of 0.034 μg $mL^{-1}$, incubated for 4 h, and washed three times with DPBS. Cells were analyzed by flow cytometry. A normalized signal intensity of 100% thereby refers to the highest observed median Cy5 signal in an individual experiment.

### 2.9. Inhibition study

Inhibitors were used to block endocytosis pathways and were added prior 100 μL 0.1 mol% DiO PS-LNP (0.28 μg mRNA $mL^{-1}$) addition (Chloropromazine (10 μg $mL^{-1}$) for 30 min, Poly I (10 μg $mL^{-1}$) for 30 min, Colchicine (10 μg $mL^{-1}$) for 2 h, Nystatin (50 μg $mL^{-1}$) for 15 min and Dynasore (80 μM) for 30 min). PS-LNPs were incubated for 4 h and washed three times with DPBS. Signal intensity of DiO expression in cells were analyzed by flow cytometry. Change in uptake was measured as a DiO signal intensity reduction of samples compared to non-inhibited median DiO signal intensity.

### 2.10. Cell viability assay

$3.3 \times 10^3$ HuH-7 cells were platted onto Collagen (Collagen I, rat tail) pre-treated clear bottom 96-multiwell plates 24 h prior transfection. An adjusted amount of sample volume compared to TE experiment with nucleic acid concentrations of 0.28 μg $mL^{-1}$ and 0.83 μg $mL^{-1}$ were added to the cells. Terfenadine (50–1 nM) was used as a negative control. After 48 h or 24 h depending on the used nucleic acid, 20 μL MTS [3-(4,5-dimethylthiazol-2-yl)-5-(3-carboxymethoxyphenyl)-2-(4-sulfophenyl)-2H-tetrazolium] reagent was added to each well and was incubated for 1 h at 37 °C and 5% $CO_2$. The absorbance was measured at 490 nm whereby the obtained results were normalized according to the

untreated cells which were defined as 100% viable.

### 2.11. Confocal laser scanning microscopy

CLSM was performed using an Olympus FV 1000 inverted microscope (Olympus Ltd, Tokyo, Japan) equipped with a 60x UPlanFLN oil immersion objective (numerical aperture 1.40). To minimize spectral cross talk, the samples were scanned using sequential mode. For confocal fluorescence and live cell imaging, HuH-7 cells were seeded into microscopy microslides (Ibidi GmbH, Gräfelfing, Germany; coated with rat tail collagen I). HuH-7 cells were incubated with LNP complexed nucleic acid at a concentration of 0.28 μg $mL^{-1}$. Cells nuclei were post-stained with Hoechst 33342 (2.5 μg $mL^{-1}$ in PBS, for 5 min). Live-Images were acquired at a controlled temperature of 37 °C using DMEM. Images were visualized by IMARIS software (Bitplane, Belfast, United Kingdom). Single-particle track speeds were analyzed using the IMARIS Tracking and Statistic Module. Spot detection was set to 0.5 μm and tracking parameters were set to autoregressive motion, max. distance = 5 μm, max gap = 3 and track duration = 120 s.

### 2.12. Zebrafish embryo (ZFE) experiments

For ZFE experiments, PEGylated LNPs were produced using the microfluidics protocol. LNPs were concentrated using an Amicon Ultra-4 centrifugal filter (10′000 molecular weight cut-off; Merck Millipore). Eggs of wildtype (abc/Tübingen) and Tg(kdrl:EGFP) adult zebrafish were collected and raised at 28 °C in 30 μg $mL^{-1}$ 1-phenyl-2-thiourea (PTU) added zebrafish culture medium. 36 h post-fertilization, ZFE were manually dechorionated and embedded in ethyl-3-aminobenzoate methanesulfonate (MS-222, Tricaine) and PTU containing 0.3% agarose. 2 × 3 nL of 75 μg $mL^{-1}$ mRNA or 150 μg $mL^{-1}$ pDNA coding for EGFP and complexed with PEGylated LNPs were intravenously injected into the Duct of Cuvier by using a micromanipulator (Wagner Instrumentenbau, Schöffengrund, Germany), a pneumatic Pico Pump PV830 (WPI, Sarasota, FL) and a Leica S8APO microscope (Leica, Wetzlar, Germany). Successfully injected ZFE were transferred into 28 °C PTU containing zebrafish culture medium. Injected ZFE were imaged between 30 and 62 h post-injection (hpi) using an Olympus FV 1000 inverted laser scanning microscope (Olympus, Tokyo, Japan) equipped with a 30x objective (UPIanSApo, 1.05NA). ZFE images were stitched using the Grid-collection stitching plug-in semi-quantitative analysis was done using a threshold in Fiji 2.1.0/1.53c software. Fluorescent signals were analyzed in the tail region of the ZFE to monitor circulating particles only [33,34]. Image were assembled in OMERO software 5.4.10 (University of Dundee & Open Microscopy Environment). To reduce intraexperimental variability, comparative experiments were performed during the same day by the same operator and using the same stage. Reproducibility was verified by repeating series of experiments on at least three different days. For each condition of each series of experiments at least 9 ZFE were used (n = 9). For the preparation of Figures and the corresponding semi-quantitative analysis, data from one representative series of experiments were used [34].

For biodistribution studies, 2 × 3 nL of 75 μg $mL^{-1}$ pDNA coding for EGFP DiI fluorescent labelled LNPs were injected into wild type ZFE and imaged from 2 to 11 hpi with a time interval of 1 h. For vasculature localization studies, Tg(kdrl:EGFP) were injected with 2 × 3 nL of 75 μg $mL^{-1}$ mRNA DiI fluorescently labelled LNPs and were imaged 4 hpi. To determine Dil PS-LNP – vasculature association, the IMARIS manual surface, measurement point and statistic modules was used. DiI PS-LNP signal within a distance of 0.5 μm and −6 μm to the EGFP vasculature signal, was defined to be associated with it.

### 2.13. Statistical analysis

If not otherwise indicated, data values are means ± SD, n = 3 independent sets of experiments. Groups were compared by ANOVA followed by Tukey post-hoc test. Analyses were performed with OriginPro 2021 software (OriginLab, Northampton, MA).

## 3. Results and discussion

### 3.1. Physico-chemical characterization of PS-LNPs

During the initial step of PS-LNP development and *in vitro* evaluation, we incorporated PS into first and second-generation LNPs by changing the lipid composition of LNPs. First generation LNPs were formulated using the permanently charged lipid DOTAP (Dioleoyl-3-trimethylammonium-propane), while the second-generation LNPs contained the ionizable lipid DODMA (1,2-dioleyloxy-3-(dimethylamino)propane), which is characterized by a $pK_a$ of 7.0 [5]. We tested different helper lipid compositions (PS, DOPC (1,2-dioleoyl-*sn*-glycerol-3-phosphocholine) and Cholesterol) while using a constant amount (50 mol%) of either DOTAP or DODMA. These lipid formulations served to condense both plasmid DNA (pDNA) and messenger RNA (mRNA) encoding for enhanced green fluorescence protein (EGFP). Formulations were prepared by a time-efficient bulk mixing method, which is amendable to formulation screening [32]. However, our protocol does not support the use of PEGylated lipids and was therefore applied for *in vitro* screening experiments only. It was the aim of these screening experiments to identify the most promising formulations. One cell line was used (HuH-7) and loading efficiency was verified to be in the range of 50% to 100%, which was sufficient for decision making during the screening process. A total of 36 formulations were thus characterized by a combination of dynamic light scattering and ζ-potential measurements. Data for N/P 6 (DOTAP) and N/P 10 (DODMA) are shown in Table 1. Since PS carries a net negative charge, we were interested in its effects on nucleic acid condensation [35,36]. At N/P 6, LNPs formulated with the permanently charged lipid DOTAP condensed nucleic acids in presence of up to 10% PS. LNPs formulated with DODMA required an increased N/P ratio of 10 to reach encapsulation efficiencies (EE) of above 50% at all tested PS concentrations. Of note, mRNA EE seemed to be lower as compared to pDNA EE, which can be attributed to different nucleic acid topologies [37]. The latter study suggests that surface potentials of DNA or RNA differ, leading to a different binding and surface distribution of ions.

Our results demonstrate that PS containing LNPs with defined physico-chemical properties can be prepared using a simple bulk mixing protocol. LNPs used in the present study had a monodisperse size distribution (PDI ≤ 0.2) and a $D_H$ in the range of 120 to 170 nm, regardless of the encapsulated nucleic acid. This is important since *in vitro* and *in vivo* interactions of nanoparticles with biological systems critically depend on particle size. Clathrin-mediated endocytosis is typically observed for particles with a size of 120–150 nm and an upper size limit of 200 nm [38]. Extravasation of macromolecules and nanoparticles through, for example, the sinusoids of the liver into the space of Disse is limited by the size of the endothelial fenestrae of 100 to 175 nm [39]. Mechanisms of cellular uptake are discussed below. A slight but not significant increase in $D_H$ distribution was obtained when LNPs were incubated with fetal calf serum (Supplementary Fig. 1). This can be attributed to the previously described interaction of non-PEG LNPs with serum proteins [40]. However, no detrimental agglomeration and formation of large particles (>1 μm) did occur.

The apparent surface charge or ζ-potential of particles is of similar importance for internalization. A positive charge of particles favors adsorptive mediated endocytosis but leads to unspecific cell interactions and a high plasma clearance and volume of distribution *in vivo* [38]. Whereas neutral to slightly negatively charged particles lead to an increased circulation half-live. Furthermore, they are expected to be less toxic as well as more stable compared to their positively charged counterparts [41,42].

ζ-potential measurements were performed at pH 4 (i.e., a pH smaller than the pKa of the ionizable lipid DODMA) and at physiological pH. As expected, at pH 7.4, a significant reduction in surface charge was

**Table 1**
**LNP screening and physico-chemical characterization.** LNPs were prepared by bulk mixing and contained DOPC, Cholesterol, DOTAP or DODMA nucleic acid condensing lipids, nucleic acids at different N/P ratios, and different amounts of incorporated PS. pDNA: plasmid DNA, mRNA: 5′ capped messenger RNA. Values are means ± SD, n ≥ 3.

| Formulation | % PS | N/P | pDNA | | | mRNA | | |
|---|---|---|---|---|---|---|---|---|
| | | | $D_H$ [nm][a] | PDI[b] | ζ-potential [mV][c] | $D_H$ [nm][a] | PDI[b] | ζ-potential [mV][c] |
| DOTAP | 0 | 6 | 138 ± 1 | 0.06 ± 0.01 | 55 ± 8 | 122 ± 1 | 0.09 ± 0.01 | 10 ± 3 |
| | 0.5 | 6 | 129 ± 2 | 0.05 ± 0.02 | 49 ± 3 | 120 ± 1 | 0.11 ± 0.01 | 13 ± 5 |
| | 1 | 6 | 122 ± 2 | 0.04 ± 0.03 | 47 ± 4 | 125 ± 0 | 0.06 ± 0.02 | 12 ± 1 |
| | 2.5 | 6 | 137 ± 3 | 0.06 ± 0.02 | 39 ± 9 | 122 ± 1 | 0.10 ± 0.01 | 7 ± 1 |
| | 5 | 6 | 130 ± 1 | 0.07 ± 0.01 | 28 ± 2 | 134 ± 1 | 0.06 ± 0.01 | 3 ± 1 |
| | 10 | 6 | 150 ± 1 | 0.13 ± 0.01 | 35 ± 1 | 147 ± 1 | 0.10 ± 0.01 | 8 ± 1 |
| DODMA | 0 | 10 | 126 ± 1 | 0.10 ± 0.02 | 21 ± 1 | 134 ± 0 | 0.11 ± 0.01 | 10 ± 1 |
| | 0.5 | 10 | 141 ± 3 | 0.15 ± 0.01 | −3 ± 2 | 136 ± 1 | 0.16 ± 0.02 | 5 ± 1 |
| | 1 | 10 | 150 ± 1 | 0.13 ± 0.01 | −17 ± 3 | 138 ± 1 | 0.14 ± 0.02 | −9 ± 0 |
| | 2.5 | 10 | 136 ± 2 | 0.13 ± 0.02 | −3 ± 0 | 128 ± 1 | 0.13 ± 0.01 | −13 ± 1 |
| | 5 | 10 | 170 ± 3 | 0.11 ± 0.01 | −4 ± 1 | 135 ± 1 | 0.13 ± 0.01 | −3 ± 1 |
| | 10 | 10 | 144 ± 2 | 0.11 ± 0.02 | −6 ± 2 | 132 ± 1 | 0.13 ± 0.01 | −10 ± 1 |

[a] Hydrodynamic diameter.
[b] Polydispersity index.
[c] ζ-potential at pH 7.4.

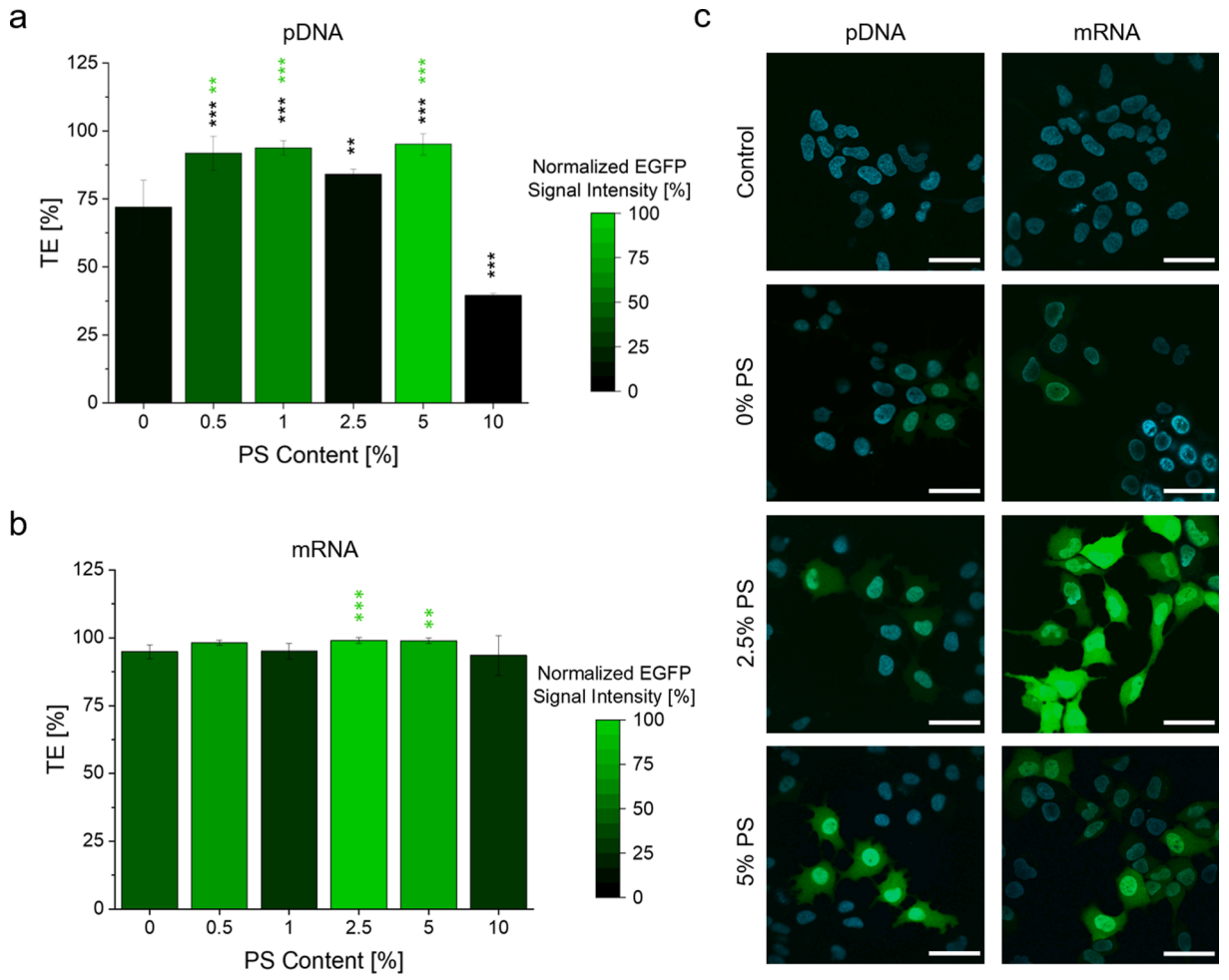


**Fig. 2.** Cellular transfection of PS-LNPs *in vitro*. Transfection efficiency (TE) and transfection potency (TP, expressed as normalized EGFP signal intensity) of HuH-7 cells treated with DODMA LNPs containing increasing amounts of incorporated PS at N/P 10. a) 0.28 μg pDNA $mL^{-1}$. 48 h incubation. b) 0.28 μg mRNA $mL^{-1}$. 24 h incubation. Values are means ± SD, n = 3. Level of significance compared to 0% PS-LNPs: *: $p \leq 0.05$, **: $p \leq 0.01$, ***: $p \leq 0.001$; Black stars: TE. Green stars: normalized EGFP signal intensity. c) Representative CLSM images of untreated control HuH-7 cells and cells treated with DODMA LNPs with 0%, 2.5%, and 5% incorporated PS. 0.28 μg nucleic acid $mL^{-1}$. Left row: pDNA and 48 h incubation. Right row: mRNA and 24 h incubation. Green signal: EGFP. Cyan signal: Hoechst 33342 nuclear stain. Scale bar: 50 μm. (For interpretation of the references to color in this figure legend, the reader is referred to the web version of this article.)

observed for DODMA based formulations. The addition of PS, which has a net charge of −1 per molecule at pH 7.4, had a direct influence on the surface charge of DODMA LNPs but no effect on nucleic acid condensation or colloidal stability. This is in contrast to previous reports using systems with different lipid compositions devoid of PS [35,36]. In presence of PS, DODMA LNPs condensing pDNA at N/P 10 a reduction from 21 ± 1 mV for 0% PS to −4 ± 1 mV for 5% PS was observed. In comparison to DODMA, DOTAP is characterized by a tertiary amine and holds a higher charge density due to its non-ionizable nature. As a consequence, an N/P ratio of 6 was sufficient to condensate nucleic acids. The ζ-potential of DOTAP LNPs with incorporated PS also decreased up to 30 mV. The resulting ζ-potentials for DOTAP PS-LNPs were still highly positive. Overall, for DODMA-based LNPs, a clear trend towards negative ζ-potentials upon addition of PS was observed. In contrast, this trend was not observed for the ζ-potential of DOTAP LNPs. At pH 4, regardless of the type of lipid, the ζ-potential was positive and approximately 30 mV (data not shown).

### 3.2. In vitro cell transfection and cell viability

Integration of PS into LNPs enhanced their ability to transfect cells *in vitro*. HuH-7 liver-derived cells were used as a cell culture model. HuH-7 cells have previously been reported to express high levels of TIM/TAM receptors and were used to study the role of PS as an apoptotic mimicry strategy of enveloped dengue and EBOLA viruses [20,43,44]. For the *in vitro* screening, EGFP encoding pDNA LNP formulations were added to cells at a final nucleic acid concentration of 0.28 μg $mL^{-1}$ or 0.83 μg $mL^{-1}$ and were analyzed by flow cytometry for LNP effectiveness i.e., transfection efficiency (TE; i.e., number of EGFP positive cells) and transfection potency (TP; i.e., mean EGFP signal intensity expressed as single-cell relative fluorescence units). While DODMA LNPs were used at an N/P ratio of 10, DOTAP LNPs had an N/P ratio of 6 due to their enhanced EE as mentioned before. These experiments revealed a strong effect of incorporated PS on the transfection ability of LNPs formulated with DODMA as well DOTAP (Fig. 2 and Supplementary Fig. 2).

These results can be summarized as follows:

First, the TE of DODMA LNPs is considerably higher than the one of DOTAP LNPs confirming previous studies [45]. In absence of PS, DOTAP containing LNPs with up to 0.83 μg $mL^{-1}$ pDNA cannot be used to transfect cells. This is in contrast to DODMA containing LNPs with 0.28 μg $mL^{-1}$ pDNA, where a high number of cells were transfected (i.e., high TE) albeit TP were low. Using mRNA complexed LNPs with mRNA concentration of 0.28 μg $mL^{-1}$ for DODMA and 0.83 μg $mL^{-1}$ for DOTAP containing LNPs showed high TE values. However, EGFP signal intensities were again low in both cases. Due to the poor performance of DOTAP LNPs, it was therefore decided to focus for the subsequent experiments on DODMA LNP formulations only.

Second, the TP of LNPs can be enhanced considerably using defined amounts of PS. Optimal results were obtained using 1 to 5% PS. Lower PS concentrations had no effect. Excessive concentrations of PS (i.e. PS content > 5%) had no or even detrimental effects as observed by a sharp decrease in TE for pDNA containing PS-LNPs. This can be attributed to the negative charge of PS interfering with pDNA condensation. With respect to DOTAP containing PS-LNPs complexed with 0.83 μg $mL^{-1}$ pDNA, cells could now be transfected using 1% PS (Supplementary Fig. 2b). However, despite the 3-fold increase of TE as well as the increased EGFP signal intensity, TP was still much weaker as compared to the DODMA containing LNPs. With respect to DODMA containing PS-LNPs, EGFP signal intensities could be considerably enhanced by a factor of three (PS-LNPs with mRNA) to six (PS-LNPs with pDNA) (Fig. 2a and b). It should be noted that TE values of DODMA mRNA-LNPs had already reached saturation, thus preventing a further increase in presence of PS. The increase in TP when incorporating PS into DODMA containing LNPs was visualized and confirmed by confocal scanning microscopy (Fig. 2c). Furthermore, as a general trend, overall TE is higher for mRNA since only the delivery to the cytoplasm is needed in contrast to pDNA, where the additive permeability barrier of the nuclear membrane has to be overcome. We conclude that PS at concentrations between 1 and 5% potentiate EGFP expression in target cells. Optimal PS concentrations to be used depend on the used nucleic acids and may vary depending on the experimental conditions.

Third, it is important to note that incorporation of PS into LNPs had no effect on cell viability as determined by the MTS assay (Supplementary Fig. 3). Of note, relatively low concentrations of all LNPs were used in the present study. We therefore observed high cell viability despite the three-fold higher concentrations and the higher ζ-potential of the DOTAP based LNPs. However, concentration dependent toxicity was not further evaluated since the focus of our attention shifted to the more promising DODMA based formulations during the course of the project.

### 3.3. Cellular uptake of PS-LNPs

Since PS promotes receptor interactions of viral and exosomal particles, we investigated if the increased TP of PS-LNPs is a consequence of enhanced cellular uptake. Therefore, PS-LNPs condensing either fluorescently labeled Cy5-pDNA or Cy5-mRNA were incubated with HuH-7 cells at a final nucleic acid concentration of 0.034 μg $mL^{-1}$ and were analyzed by flow cytometry (Fig. 3a and b). For pDNA LNPs 4 h post-incubation, only slight changes regarding the amount of Cy5 + cells were observed (>10%). Nevertheless, an almost 1.6- respectively 1.3-fold increased Cy5 signal intensity was observed for formulations with 2.5% PS and 5% PS as compared to the 0% PS formulation. A similar trend was observed using mRNA PS-LNPs. Again, Cy5 + cells could be increased by 13% using 2.5% PS-LNPs compared to 0% PS formulations, whereas 5% PS-LNPs lead to 15% fewer Cy5 + cells. Furthermore, Cy5 signal intensity increased 1.6-fold for 2.5% PS formulation, and again no significant difference for 5% PS formulations compared to 0% PS was observed. In these experiments, the amount of Cy5 + cells was lower using mRNA LNPs compared to LNPs condensing pDNA. This could be due to faster processing of mRNA LNPs since first EGFP signals were already observed after 4 h of incubation and were significantly higher for 2.5% PS compared to the other formulations. Overall it can be summarized that a well-defined amount of PS (i.e., 2.5 to 5% PS) was needed to induce cellular uptake confirming previous results.

To analyze the intracellular fate of PS-LNPs, we applied a combination of confocal laser scanning microscopy and differential interference contrast (DIC) live-cell microscopy (Fig. 3c) using fluorescently labeled PS-LNPs. Intracellular tracking of PS-LNPs reveals considerable differences between PS-LNPs and LNPs devoid of PS. Tracking of > 120 single particles containing 2.5 to 5% PS revealed a median particle speed of 0.11 ± 0.04 μm $s^{-1}$ for 2.5% PS and 0.09 ± 0.06 μm $s^{-1}$ for 5% PS, respectively. These median speeds were significantly higher than those of LNPs without PS (0.06 ± 0.05 μm $s^{-1}$) (Supplementary Figure 4). While cellular uptake of the latter lead to their accumulation at the cell periphery, a clear accumulation in the perinuclear region of PS-LNPs is observed. It remains to be elucidated if PS has a beneficial effect on intracellular processing and cytosolic liberation of nucleic acids.

Our findings thus suggest that PS-LNPs interact with target cells in a highly specific manner. To elucidate mechanisms of cellular uptake and intracellular processing in the presence and absence of PS, we conducted a series of cellular uptake inhibition experiments (Supplementary Fig. 5). An arbitrary threshold of at least 50% inhibition was considered to be significant. Uptake of PS-LNPs (in contrast to LNPs) was specifically inhibited by Annexin V (which was previously demonstrated to bind to PS and therefore blocks the uptake of apoptotic cells [46]) and by Chlorpromazine (a known clathrin-mediated endocytosis inhibitor). Uptake of both PS-LNPs and LNPs was specifically inhibited by Colchicine (inhibitor of tubulin polymerization), Dynasore (inhibition of clathrin-mediated endocytosis), and Poly I:C (a synthetic single-stranded RNA that can competitively bind to the scavenger receptor SR-A [47]). Remarkably, Poly I:C inhibited cellular uptake of LNPs by

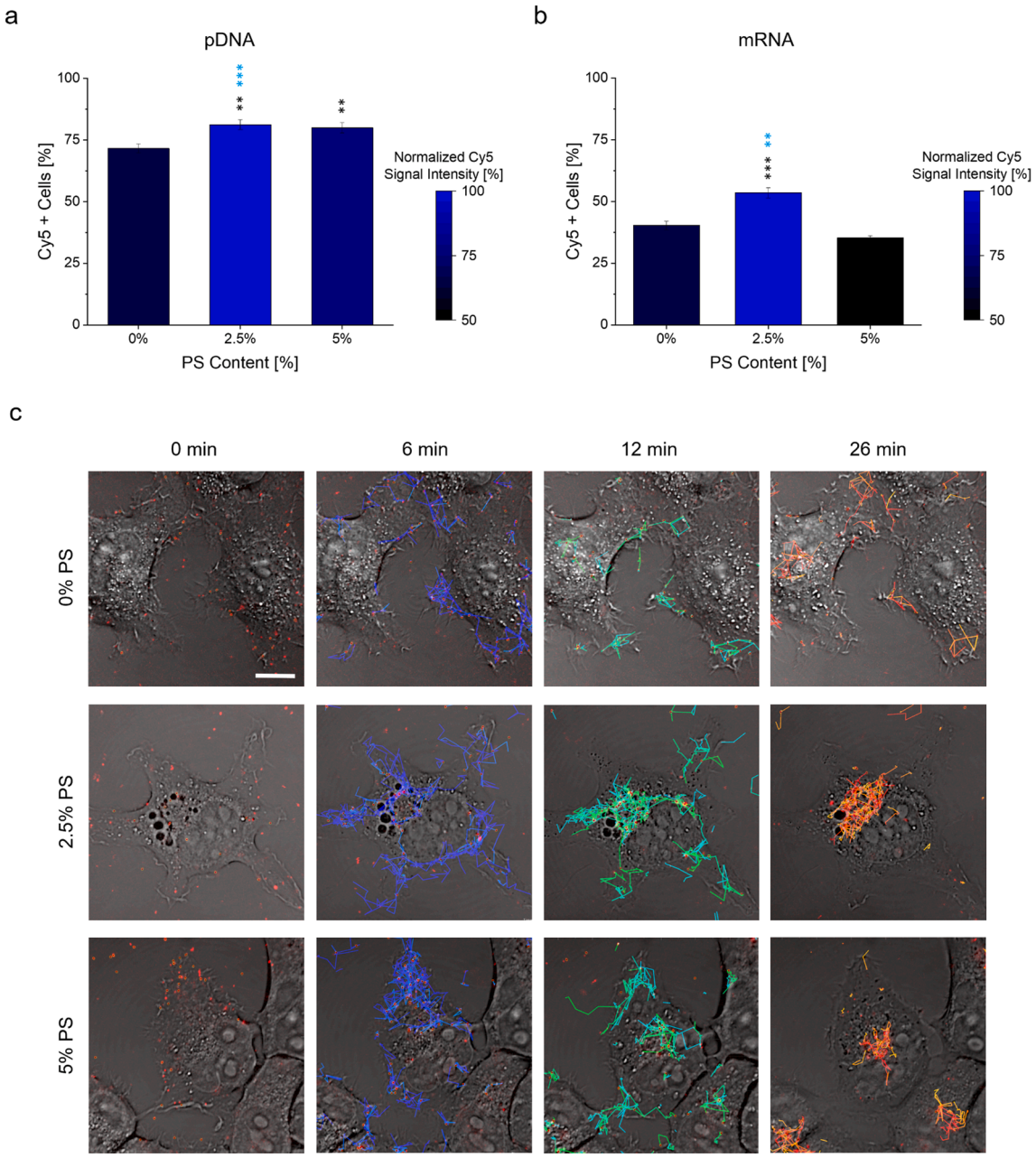


**Fig. 3.** Cellular uptake of PS-LNPs. HuH-7 cells were incubated with fluorescently labeled PS-LNPs (0 to 5% PS). Quantitation of cellular uptake of PS-LNPs condensing fluorescently labeled a) Cy5-pDNA or b) Cy5-mRNA at a final nucleic acid concentration of 0.034 μg $mL^{-1}$ by flow cytometry (N/P 10, 4 h incubation). Values are means ± SD, n = 3. Level of significance compared to 0% PS-LNPs: *: $p \leq 0.05$, **: $p \leq 0.01$, ***: $p \leq 0.001$; Black stars: Cy5 + cells. Blue stars: normalized Cy5 signal intensity. c) Representative CLSM images of DiI-PS-LNP tracking analysis (N/P 10, 0.28 μg pDNA $mL^{-1}$). Particle tracks are heat-mapped from blue (6 min) to red (26 min). Scale Bar: 10 μm. (For interpretation of the references to color in this figure legend, the reader is referred to the web version of this article.)

50% but almost completely blocked the uptake of PS-LNPs.

These experiments indicate that LNPs and PS-LNPs share cellular uptake pathways such as clathrin-mediated endocytosis, a process that depends on microtubules [48]. In addition, PS-LNPs activate PS-specific uptake mechanisms, as demonstrated by the inhibitory action of Annexin V. Our studies with Annexin V suggest that this effect contributes by 50% to the total observed cellular uptake. Interestingly, PS seems to potentiate the inhibitory effect of Poly I:C, suggesting a strong involvement of the scavenger receptor SR-A. This receptor acts as a pathogen sensor of extracellular dsRNA and recognizes a range of ligands including low density lipoproteins and nucleic acids [47,49]. Our results seem to suggest that SR-A facilitates cellular entry of LNPs and that PS facilitates this process.

### 3.4. *In vivo evaluation of PS-LNPs*

The increased ability of PS-LNP to transfect cells observed *in vitro* was verified *in vivo* using the developing zebrafish embryo (ZFE) as an *in vivo* vertebrate screening model [50]. Formulations were injected intravenously into the Duct of Cuvier of ZFE 36 h post-fertilization. In these experiments (and in contrast to the *in vitro* experiments), PS-LNPs were modified with PEGylated phospholipids (i.e., DMPE-PEG2000). This modification is necessary to suppress opsonization and agglomeration in presence of plasma protein. In addition, immune interactions

can be suppressed such as inflammatory reactions or recognition of LNPs by cells of the mononuclear phagocyte system [51]. Since PEGylation interferes with the condensation of nucleic acids, these LNPs were prepared using a microfluidics protocol [52] and not bulk mixing. PEGylated LNPs were characterized by a mean $D_H$ of approximately 105 nm and a monodisperse PDI of 0.15 (Supplementary Table 1). PEGylated LNPs have a slightly lower surface charge at physiological pH as compared to their non-PEGylated counterparts with values in the range of −3 mV to −12 mV. This is indicative of the shielding of the negative charge of PS by DMPE-PEG2000. The EE was in the range of 87–100% for pDNA and 54–78% for mRNA. For all *in vivo* studies, the same amounts of nucleic acids were administered (i.e., 6 nL injection volume, 75 μg $mL^{-1}$ mRNA, 150 μg $mL^{-1}$ pDNA).

*In vivo* experiments in ZFE confirmed our *in vitro* results (Fig. 4). In our study, we have focused on an analysis of the ZFE tail region in the vicinity of the caudal vein since this tissue, but not the teleost liver, harbors macrophages, and scavenger endothelial cells. It can therefore be considered to have the same functionality as the mammalian liver sinusoids [53]. Furthermore, the head region of the ZFE was excluded from analysis since passive trapping of particles within the ocular vasculature cannot be excluded. As expected and in agreement with previous *in vitro* results, free nucleic acids or LNPs devoid of PS show minimal activity 42 h post-injection (hpi). The addition of PS to pDNA-LNPs led to 1.3-fold enhanced EGFP expression in the tail region of the ZFE compared to 0% PS formulation. In contrast, the addition of PS to mRNA-LNPs resulted in a strong and widely distributed EGFP signal throughout the ZFE, leading to a 3.7-fold increased TP (Fig. 4b). A semi-quantitative analysis of the tail region of the ZFE revealed 3.2-fold versus 5.2-fold increase in TE between pDNA PS-LNP and mRNA PS-LNP treated ZFE compared to 0% PS formulations. It can be concluded that PS enhances TE for both types of LNPs, however, to a higher extent for mRNA-LNPs as compared to pDNA-LNP. Even though the evaluation of TP reveals less pronounced differences, the same trends are observed. Concerning the biodistribution of LNPs, we observed an increased EGFP signal in the tail region for PS containing LNP formulations. This distribution pattern is indicative of PS-LNP deposition in the ZFE tail vasculature which could be localized starting from 4 to 8 hpi. Semi-quantitative image analysis of confocal image stacks revealed enhanced extravasation and penetration of PS-LNPs into tissues surrounding the vasculature (Fig. 4c). In these experiments, 62% ± 4% of DiI PS-LNP signal was associated with the ZFE vasculature. This is in contrast to LNPs devoid of PS (Supplementary Fig. 6), which were retained to a higher degree within the vasculature (46% ± 9% association). These interactions with the vasculature are similar to the previously reported biodistribution of PS marked exosomes and negatively charged liposomes [54]. Overall no toxic effects were observed in ZFE after LNP administration.

## 4. Conclusion

In the present study, we could demonstrate that the biomimetic incorporation of PS into LNPs enhances transfection efficiency and transfection potency *in vitro* as well as *in vivo*. Furthermore, PS-LNPs have a distinct intracellular mobility, which is similar to enveloped viruses, exosomes, and PS equipped liposomes. PS enhances interactions with scavenger receptors of target cells leading to an enhanced cellular uptake by clathrin-mediated endocytosis. PS enhances the transfection efficiency and transfection potency of both pDNA and mRNA based LNPs. Further optimization of PS-LNPs can presumably be achieved by the use of more complex viral-like compositions [31]. Additional studies will focus on the beneficial anti-inflammatory and tolerogenic effects of PS [55] when combined with LNPs. The incorporation of the bioactive

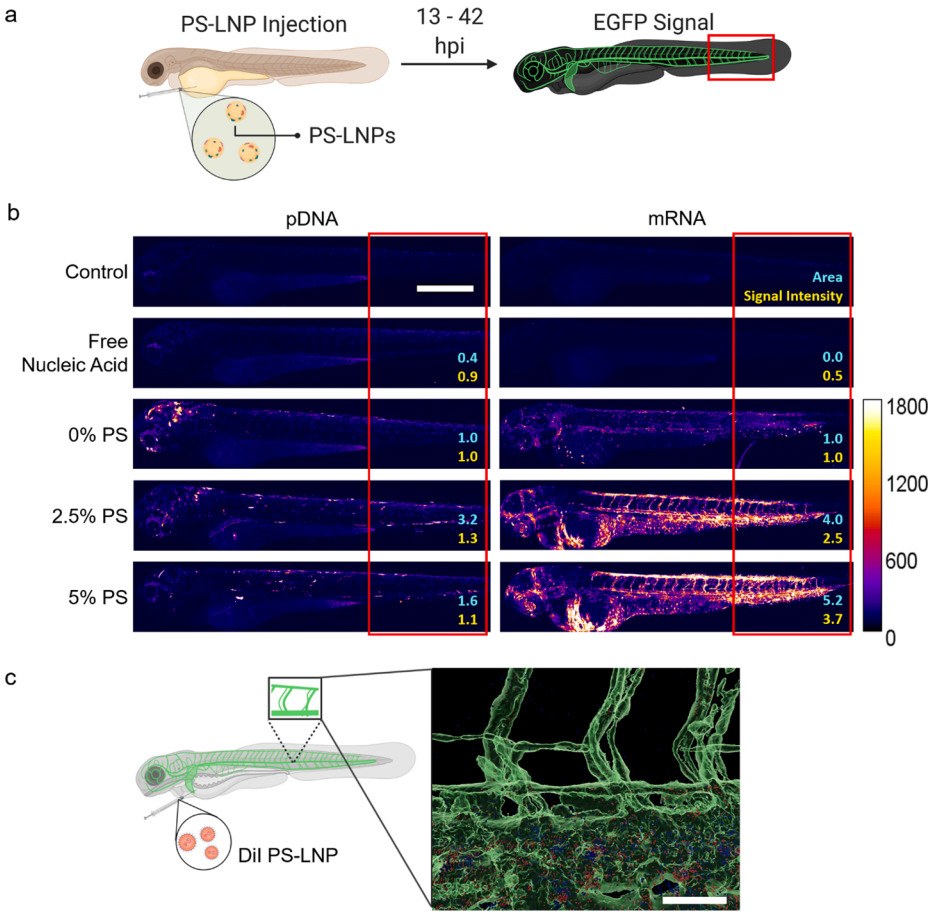


**Fig. 4.** *In vivo* evaluation of PS-LNP uptake and transfection in the zebrafish embryo (ZFE). Transfection efficiency (TE), transfection potency (TP), and biodistribution of LNPs were studied using ZFE. a) Schematic representation of the experimental procedure. After intravenous injection of LNPs, EGFP signal were visualized by CLSM within 13 hpi (for mRNA) to 42 hpi (for pDNA). Red: area of interest. b) Representative CLSM images of ZFE injected with PS-LNPs condensing either EGFP coding pDNA or mRNA. Color-coding according to EGFP signal intensity. Cyan: TE-fold difference as compared to 0% PS formulation; Yellow: TP-fold difference as compared to 0% PS formulation. Scale Bar: 100 μm. c) Representative 3D-rendered image of a ZFE Tg(kdrl:EGFP) injected with DiI-labeled 2.5% PS-LNPs condensing pDNA. ZFE were analyzed 4 hpi. Green signal: ZFE vasculature, Red signal: DiI PS-LNPs associated with ZFE vasculature, Blue signal: DiI PS-LNPs not associated with ZFE vasculature. Scale Bar: 50 μm. (For interpretation of the references to color in this figure legend, the reader is referred to the web version of this article.)

lipid PS in LNPs is a promising strategy to enhance the efficacy of gene delivery systems and can serve for enhancement of other delivery systems by the decoration of the carriers.

## 5. Ethical regulations

Animals were maintained according to Swiss animal welfare regulations and were handled according to approved institutional animal care and use protocols of the University of Basel.

## Declaration of Competing Interest

The authors declare that they have no known competing financial interests or personal relationships that could have appeared to influence the work reported in this paper.

## Data availability statement

Supporting and raw data is included in the Supplementary Materials or can be retrieved from the public data repository Zenodo (https://zenodo.com).

*Acknowledgment*

The authors thank Dr. S. Schenk (University of Basel) for providing valuable scientific advice and support. We thank Dr. K. Schleicher (Imaging Core Facility, University of Basel) for his valuable help with imaging processing and analysis. We thank Prof. Dr. M. Affolter and Dr. H.G. Belting for providing zebrafish eggs. Furthermore, the authors acknowledge Nicole Rimann (University Children's Hospital Zurich) for the supply with pDNA. Schemes were created using BioRender.com.

*Funding*

This work was supported by the Swiss Nanoscience Institute (Grant P1801), the Swiss National Science Foundation (Sinergia Grant CRSII5_180257), and the Phospholipid Research Center Heidelberg (Grant JHU-2021-094/2-1).

*Author contributions*

J.H., T.E., C.L., C.A. contributed to the apoptotic cell mimicry LNP concept, experiment planning, and writing the manuscript. C.L. and C.A. contributed equally to LNP formulation, characterization, tissue-culture work, and ZFE work. J.B. contributed to ZFE experiments. P.D. and C.P. contributed to the experimental design and editing of the manuscript.

## Appendix A. Supplementary data

Supplementary data to this article can be found online at https://doi.org/10.1016/j.ejpb.2022.02.007.

## References

[1] A. Akinc, et al., The Onpattro story and the clinical translation of nanomedicines containing nucleic acid-based drugs, Nat. Nanotechnol. 14 (2019) 1084–1087.
[2] J. Buck, P. Grossen, P.R. Cullis, J. Huwyler, D. Witzigmann, Lipid-Based DNA Therapeutics: Hallmarks of Non-Viral Gene Delivery, ACS Nano 13 (4) (2019) 3754–3782.
[3] M.J. Stewart, et al., Gene Transfer In Vivo with DNA–Liposome Complexes: Safety and Acute Toxicity in Mice, Hum. Gene Ther. 3 (1992) 267–275.
[4] H. San, et al., Safety and Short-Term Toxicity of a Novel Cationic Lipid Formulation for Human Gene Therapy, Hum. Gene Ther. 4 (1993) 781–788.
[5] J. Heyes, L. Palmer, K. Bremner, I. MacLachlan, Cationic lipid saturation influences intracellular delivery of encapsulated nucleic acids, J. Controlled Release 107 (2) (2005) 276–287.
[6] S.C. Semple, S.K. Klimuk, T.O. Harasym, M.J. Hope, Lipid-based formulations of antisense oligonucleotides for systemic delivery applications, in: Methods in Enzymology, vol. 313, Academic Press, 2000, pp. 322–341.
[7] A. Akinc, et al., A combinatorial library of lipid-like materials for delivery of RNAi therapeutics, Nat. Biotechnol. 26 (2008) 561–569.
[8] C.D. Sago, et al., High-throughput in vivo screen of functional mRNA delivery identifies nanoparticles for endothelial cell gene editing, Proc. Natl. Acad. Sci. 115 (2018) E9944–E9952.
[9] Y. Xia, J. Tian, X. Chen, Effect of surface properties on liposomal siRNA delivery, Biomaterials 79 (2016) 56–68.
[10] A. Akinc, M. Goldberg, J. Qin, J.R. Dorkin, C. Gamba-Vitalo, M. Maier, K. N. Jayaprakash, M. Jayaraman, K.G. Rajeev, M. Manoharan, V. Koteliansky, I. Röhl, E.S. Leshchiner, R. Langer, D.G. Anderson, Development of lipidoid-siRNA formulations for systemic delivery to the liver, Mol. Ther. J. Am. Soc. Gene Ther. 17 (5) (2009) 872–879.
[11] J. Kim, A. Jozic, G. Sahay, Naturally Derived Membrane Lipids Impact Nanoparticle-Based Messenger RNA Delivery, Cell. Mol. Bioeng. 13 (2020) 463–474.
[12] S. Patel, et al., Naturally-occurring cholesterol analogues in lipid nanoparticles induce polymorphic shape and enhance intracellular delivery of mRNA, Nat. Commun. 11 (2020) 1–13.
[13] J.A. Kulkarni, et al., Design of lipid nanoparticles for in vitro and in vivo delivery of plasmid DNA, Nanomed. Nanotechnol. Biol. Med. 13 (2017) 1377–1387.
[14] X. Cheng, R.J. Lee, The role of helper lipids in lipid nanoparticles (LNPs) designed for oligonucleotide delivery, Adv. Drug Deliv. Rev. 99 (2016) 129–137.
[15] Q. Cheng, et al., Selective organ targeting (SORT) nanoparticles for tissue-specific mRNA delivery and CRISPR–Cas gene editing, Nat. Nanotechnol. 15 (2020) 313–320.
[16] P.T. Ivanova, et al., Lipid composition of viral envelope of three strains of influenza virus – not all viruses are created equal, ACS Infect. Dis. 1 (2015) 399–452.
[17] K. Morizono, I.S.Y. Chen, Role of Phosphatidylserine Receptors in Enveloped Virus Infection, J. Virol. 88 (2014) 4275–4290.
[18] J. Wang, L. Qiao, Z. Hou, G. Luo, J.-H. Ou, TIM-1 Promotes Hepatitis C Virus Cell Attachment and Infection, J. Virol. 91 (2) (2017), https://doi.org/10.1128/JVI.01583-16.
[19] B. Brunton, et al., TIM-1 serves as a receptor for Ebola virus in vivo, enhancing viremia and pathogenesis, PLoS Negl. Trop. Dis. 13 (2019).
[20] L.-W. Chu, C.-J. Yang, K.-J. Peng, P.-L. Chen, S.-J. Wang, Y.-H. Ping, TIM-1 As a Signal Receptor Triggers Dengue Virus-Induced Autophagy, Int. J. Mol. Sci. 20 (19) (2019) 4893, https://doi.org/10.3390/ijms20194893.
[21] A. Amara, J. Mercer, Viral apoptotic mimicry, Nat. Rev. Microbiol. 13 (8) (2015) 461–469.
[22] A.C. Doran, A. Yurdagul, I. Tabas, Efferocytosis in health and disease, Nat. Rev. Immunol. 20 (4) (2020) 254–267, https://doi.org/10.1038/s41577-019-0240-6.
[23] E. Boada-Romero, J. Martinez, B.L. Heckmann, D.R. Green, The clearance of dead cells by efferocytosis, Nat. Rev. Mol. Cell Biol. 21 (7) (2020) 398–414.
[24] S.P. Davies, G.M. Reynolds, Z. Stamataki, Clearance of Apoptotic Cells by Tissue Epithelia: A Putative Role for Hepatocytes in Liver Efferocytosis, Front. Immunol. 9 (2018).
[25] J.C. Seeberg, et al., Non-professional phagocytosis: a general feature of normal tissue cells, Sci. Rep. 9 (2019) 11875.
[26] M.B. Naeini, V. Bianconi, M. Pirro, A. Sahebkar, The role of phosphatidylserine recognition receptors in multiple biological functions, Cell. Mol. Biol. Lett. 25 (1) (2020), https://doi.org/10.1186/s11658-020-00214-z.
[27] J.L.M. Wanderley, R.A. DaMatta, M.A. Barcinski, Apoptotic mimicry as a strategy for the establishment of parasitic infections: parasite- and host-derived phosphatidylserine as key molecule, Cell Commun. Signal. 18 (2020) 10.
[28] A. Matsumoto, et al., Role of Phosphatidylserine-Derived Negative Surface Charges in the Recognition and Uptake of Intravenously Injected B16BL6-Derived Exosomes by Macrophages, J. Pharm. Sci. 106 (2017) 168–175.
[29] X. Wei, et al., Surface Phosphatidylserine Is Responsible for the Internalization on Microvesicles Derived from Hypoxia-Induced Human Bone Marrow Mesenchymal Stem Cells into Human Endothelial Cells, PLOS ONE 11 (2016) e0147360.
[30] Z. Yao, Y. Qiao, X. Li, J. Chen, J. Ding, L.u. Bai, F. Shen, B. Shi, J. Liu, L.u. Peng, J. Li, Z. Yuan, R.M. Sandri-Goldin, Exosomes Exploit the Virus Entry Machinery and Pathway To Transmit Alpha Interferon-Induced Antiviral Activity, J. Virol. 92 (24) (2018), https://doi.org/10.1128/JVI.01578-18.
[31] S. Pollock, et al., Uptake and trafficking of liposomes to the endoplasmic reticulum, FASEB J. Off. Publ. Fed. Am. Soc Exp. Biol. 24 (2010) 1866–1878.
[32] J. Buck, D. Mueller, U. Mettal, M. Ackermann, H.M. Grisch-Chan, B. Thöny, A. Zumbuehl, J. Huwyler, D. Witzigmann, Improvement of DNA Vector Delivery of DOTAP Lipoplexes by Short-Chain Aminolipids, ACS Omega 5 (38) (2020) 24724–24732.
[33] S. Sieber, P. Grossen, P. Detampel, S. Siegfried, D. Witzigmann, J. Huwyler, Zebrafish as an early stage screening tool to study the systemic circulation of nanoparticulate drug delivery systems in vivo, J. Control. Release 264 (2017) 180–191.
[34] J.S. Bolten, A. Pratsinis, C.L. Alter, G. Fricker, J. Huwyler, Zebrafish (Danio rerio) larva as an in vivo vertebrate model to study renal function, Am. J. Physiol.-Ren. Physiol. (2022), https://doi.org/10.1152/ajprenal.00375.2021.
[35] A.L. Bailey, P.R. Cullis, Membrane Fusion with Cationic Liposomes: Effects of Target Membrane Lipid Composition †, Biochemistry 36 (1997) 1628–1634.
[36] F.C. Tsui, D.M. Ojcius, W.L. Hubbell, The intrinsic pKa values for phosphatidylserine and phosphatidylethanolamine in phosphatidylcholine host bilayers, Biophys. J. 49 (1986) 459–468.
[37] L. Li, S.A. Pabit, S.P. Meisburger, L. Pollack, Double-stranded RNA resists condensation, Phys. Rev. Lett. 106 (2011), 108101.

[38] H. Kettiger, A. Schipanski, P. Wick, J. Huwyler, Engineered nanomaterial uptake and tissue distribution: from cell to organism, Int. J. Nanomedicine 8 (2013) 3255–3269.
[39] F. Braet, E. Wisse, Structural and functional aspects of liver sinusoidal endothelial cell fenestrae: a review, Comp. Hepatol. 1 (2002) 1.
[40] V. Francia, R.M. Schiffelers, P.R. Cullis, D. Witzigmann, The Biomolecular Corona of Lipid Nanoparticles for Gene Therapy, Bioconjug. Chem. 31 (2020) 2046–2059.
[41] M.J. Mitchell, et al., Engineering precision nanoparticles for drug delivery, Nat. Rev. Drug Discov. 20 (2021) 101–124.
[42] S. Martins, et al., Solid lipid nanoparticles as intracellular drug transporters: An investigation of the uptake mechanism and pathway, Int. J. Pharm. 430 (2012) 216–227.
[43] L. Meertens, X. Carnec, M. Lecoin, R. Ramdasi, F. Guivel-Benhassine, E. Lew, G. Lemke, O. Schwartz, A. Amara, The TIM and TAM Families of Phosphatidylserine Receptors Mediate Dengue Virus Entry, Cell Host Microbe 12 (4) (2012) 544–557.
[44] A.S. Kondratowicz, et al., T-cell immunoglobulin and mucin domain 1 (TIM-1) is a receptor for Zaire Ebolavirus and Lake Victoria Marburgvirus, Proc. Natl. Acad. Sci. 108 (2011) 8426–8431.
[45] A.K.K. Leung, Y.Y.C. Tam, P.R. Cullis, Lipid Nanoparticles for Short Interfering RNA Delivery, Adv. Genet. 88 (2014) 71–110.
[46] V.A. Fadok, et al., Exposure of phosphatidylserine on the surface of apoptotic lymphocytes triggers specific recognition and removal by macrophages, J. Immunol. 148 (1992) 2207–2216.
[47] G.V. Limmon, et al., Scavenger receptor class-A is a novel cell surface receptor for double-stranded RNA, FASEB J. Off. Publ. Fed. Am. Soc Exp. Biol. 22 (2008) 159–167.
[48] A. Kakigi, et al., Actin filaments and microtubules regulate endocytosis in marginal cells of the stria vascularis, Acta Otolaryngol. (Stockh.) 128 (2008) 856–860.
[49] E. Pandey, A.S. Nour, E.N. Harris, Prominent Receptors of Liver Sinusoidal Endothelial Cells in Liver Homeostasis and Disease, Front. Physiol. 11 (2020) 873.
[50] S. Sieber, P. Grossen, J. Bussmann, F. Campbell, A. Kros, D. Witzigmann, J. Huwyler, Zebrafish as a preclinical in vivo screening model for nanomedicines, Adv. Drug Deliv. Rev. 151-152 (2019) 152–168, https://doi.org/10.1016/j.addr.2019.01.001.
[51] P.L. Turecek, M.J. Bossard, F. Schoetens, I.A. Ivens, PEGylation of Biopharmaceuticals: A Review of Chemistry and Nonclinical Safety Information of Approved Drugs, J. Pharm. Sci. 105 (2016) 460–475.
[52] M. Sedighi, et al., Rapid optimization of liposome characteristics using a combined microfluidics and design-of-experiment approach, Drug Deliv. Transl. Res. 9 (2019) 404–413.
[53] F. Campbell, F.L. Bos, S. Sieber, G. Arias-Alpizar, B.E. Koch, J. Huwyler, A. Kros, J. Bussmann, Directing Nanoparticle Biodistribution through Evasion and Exploitation of Stab2-Dependent Nanoparticle Uptake, ACS Nano 12 (3) (2018) 2138–2150.
[54] F.J. Verweij, C. Revenu, G. Arras, F. Dingli, D. Loew, D.M. Pegtel, G. Follain, G. Allio, J.G. Goetz, P. Zimmermann, P. Herbomel, F. Del Bene, G. Raposo, G. van Niel, Live Tracking of Inter-organ Communication by Endogenous Exosomes In Vivo, Dev. Cell 48 (4) (2019) 573–589.e4.
[55] M. Darabi, A. Kontush, Phosphatidylserine in atherosclerosis, Curr. Opin. Lipidol. 27 (4) (2016) 414–420.